J Mater Sci (2018) 53:8989–9001

Composites

Sintering and tribomechanical properties of gel-combustion-derived nano-alumina and its composites with carbon nanotubes

Rupa Halder[1], Soumya Sarkar[1], Siddhartha Bandyopadhyay[1,*], and Pravash C. Chakraborti[2]

[1] CSIR- Central Glass and Ceramic Research Institute, 196, Raja S.C. Mullick Road, Kolkata 700 032, India
[2] Metallurgical and Material Engineering, Jadavpur University, Kolkata 700032, India

Received: 23 August 2017
Accepted: 28 February 2018
Published online: 9 March 2018

ABSTRACT

Fully pure nano-α-alumina (Al_2O_3) was prepared following gel-combustion method. Near theoretically dense monolithic Al_2O_3 and its composites reinforced with multiwalled carbon nanotubes (MWCNTs) were prepared using spark plasma sintering (SPS) at 1500 °C under 40 MPa within 10 min. The shrinkage curves were guided in sequence by the crystallization of the amorphous mass followed by a solid-state sintering. The differential nature of electrical conductivity of both composite phases resulted in enhanced densification through localized joule heating. Formation of ~ 1-μm-sized equiaxed matrix grains with uniform distribution of structurally survived CNTs in it was observed in the sintered composites. Within the investigated loading span, the highest Vickers hardness (H_V) values were obtained only at 0.5 wt% MWCNT loading in matrix Al_2O_3. Improvements in H_V values for the composites at 0.2 and 2 kgf indentation loads were found to be ~ 18 and ~ 12%, respectively, in comparison with those obtained for pure matrix phase. Quantitative indentation size effect analyzed through standard mathematical models indicated the role of matrix grain refinement and proper matrix–filler load sharing in changing the true hardness. On the contrary, increased CNT concentration leaded to increased sensitivity toward size effect due to the extreme flexible nature of the filler. Unlubricated linear scratch experiments revealed ~ 30–45% lower specific wear rate (W_R) values of the composite specimens compared to SPS-processed monolithic Al_2O_3. Microstructure and scar profile observations were utilized to describe such enhanced wear resistance of present composites.

Address correspondence to E-mail: sbando@cgcri.res.in

https://doi.org/10.1007/s10853-018-2187-6

Introduction

Owing to the suitable combination of material properties at a reasonable price, Al_2O_3 ceramics with purity in the range of 85–99.999% have been widely utilized in various sectors satisfying traditional to advanced needs starting from production of aluminum metal, catalysts, high-frequency insulators, substrates for electronic circuits, abrasives, cutting tools, nozzles, seals, kiln furniture to biomedical implants, ceramic armors and missile radomes [1–5]. On the contrary, extensive brittleness and limited toughness sometimes limit its applicability in high-performance sectors. Thus, to impart improved toughness and resistance to catastrophic failure to monolithic Al_2O_3, research work on compositing with suitable reinforcing filler in the form of either particulate or fiber has been going on globally since long back [6]. In recent years, researchers are also trying to improve mechanical performance of structural Al_2O_3 through CNT incorporation due to fascinating mechanical properties of the nanotubes as reinforcing phase [7–12]. However, challenges still exist in fabricating effective CNT/Al_2O_3 composites which can offer properties better than pure Al_2O_3 and researchers are meticulously trying to overcome such issues to fabricate efficient CNT/Al_2O_3 composites suitable for high-performance applications. As far as property evaluation is concerned, tribological performance evaluation of CNT/Al_2O_3 composites is still limited and, thus, needs much attention prior to real-life application [10, 13–15]. In this work, an attempt was made to fabricate MWCNT/Al_2O_3 composites under spark plasma processing using in-house gel-combustion-synthesized fully pure nano-sized α-Al_2O_3 powder as the source for matrix phase and 0.25 and 0.5 wt% commercial MWCNT as reinforcement. Sintering behaviors of both monolith and composites were studied in detail. The specimens were characterized in terms of Vickers hardness (H_V) within 0.2 and 2 kgf indentation load and unlubricated wear performance under normal loads (F_N) of 10 and 20 N to assess the effect of CNT incorporation in Al_2O_3 matrix. Indentation size effect (ISE) analyses of H_V data were performed using three well-established mathematical models. Wear behavior of the specimens was discussed in terms of coefficient of friction (COF, μ) and specific wear rate (W_R) values and with the help of formed microstructure and scar profile features.

Materials and methods

Combustion synthesis of nano-α-Al_2O_3

Commercially available chemical reagents, like aluminum (M^+) nitrate nonahydrate [Merck, India], urea (U) [Merck, India], formaldehyde solution (F) [37% (w/v), Merck, India], ammonia solution [of 25% grade, Merck, India], were used for the synthesis of α-alumina. In the first step, urea and formaldehyde solution were mixed and the mixture was left for 24 h for proper digestion to make methylol urea. In the next step, aluminum nitrate salt and additional urea were added to methylol urea to prepare a stoichiometric (M^+/U/F = 1:2:4) mixture. The mixture transformed into gel within few minutes. The gel was dried in oven at 120 °C. After complete drying, the gel was ignited with the help of an externally burning match stick. The self-propagating reactions from different steps of cracking of the resin keep progressing spontaneously; those ultimately produce soft fluffy powder at the end of the burning process [16]. The as-synthesized powder was white to occasionally light brownish. The brownish color was because of some small fraction of unburnt remnant polymer in the product. The powder was heat-treated at 1100 °C for 30 min under flowing dry air to produce partly crystallized variety of pure α-Al_2O_3. Morphologies of the heat-treated powder were viewed through a field emission scanning electron microscope (FESEM, Supra-35, VP-Carl Zeiss, Germany) and transmission electron microscope (TEM, Tecnai G2 30ST, FEI Company, Netherlands).

SPS processing of combustion-synthesized nano-α-Al_2O_3 and MWCNT/α-Al_2O_3 composites

The combustion-synthesized pure nano-α-Al_2O_3 (particle size: as described in later "Morphological characteristics of synthesized alumina" section) and commercial MWCNT (purity ~ 95 wt%, outer diameter 30–50 nm, length 10–20 μm, SRL Pvt. Ltd., India) were mixed thoroughly using probe sonication in isopropyl alcohol for 1 h. The mixed slurry was then dried at ~ 75 °C. Two powder mixtures having 0.25 and 0.5 wt% MWCNT loading (nomenclatured as A 0.25 and A 0.5, respectively, in tables and figures) were prepared using the above procedure. The pure α-Al_2O_3 (referred to as A in tables and figures) and the composite powder mixtures were then

consolidated at 1500 °C with 10 min of dwell time under 40 MPa in a Spark Plasma Sintering furnace (SPS, FCT Systeme GmbH, Germany) using heating and cooling rates of 25 and 10 °C/min, respectively. A gaseous atmosphere of argon was used during sintering. The sintering was performed using pulsed DC (T_{on} = 10 ms; T_{off} = 2 ms). To check the structural stability of MWCNT after SPS processing, the as-received MWCNT was also compacted using the same sintering schedule. Morphologies of both as-received and heat-treated CNTs were viewed under FESEM.

Characterizations of the sintered specimens

Bulk density (BD) values of the specimens were measured using Archimedes water immersion technique. The sintered specimens were ground and polished using a diamond grinding–polishing machine (Tegramin 30, Struers, Denmark) with 40–0.25-μm diamond grits in sequential steps. Surface roughness values (R_a) of the polished samples were measured using a non-contact-type surface profilometer (Contour GT, M/s Bruker, USA). A micro-Vickers hardness tester (402 MVD, M/s Wolpert Wilson, Germany) was used to evaluate hardness values of the specimens at five indentation loads from 0.2 to 2 kgf with 10 s dwell. 10–15 indents were made on each of the specimens at each of the test loads for averaging purpose. Unlubricated room temperature linear scratch tests were conducted in TR-101 Tribometer (DUCOM, India) using a diamond Vickers indenter under two normal loads, i.e., 10 and 20 N keeping scratching length (L) and speed constant at 3 mm and 0.1 mm/s, respectively. COF and W_R values were calculated using standard expressions [10]. Scar profiles were viewed through the surface profilometer and a desktop scanning electron microscope (SEM; proX, Phenom World BV, The Netherlands) for dimensional and morphological analyses of the worn tracks, respectively.

Results and discussion

Morphological characteristics of synthesized alumina

Figure 1a–d shows various features of the gel-combustion-synthesized α-Al_2O_3 powder. The FESEM image (Fig. 1a) indicates the presence of clustered nano-sized α-Al_2O_3 grains containing individual grains of 30–70 nm. Figure 1b confirms the characteristic presence of aluminum (Al) and oxygen (O) in the synthesized grains and absolute absence of any other impurity elements. The carbon (C) peak in the EDX pattern appeared from the carbonaceous conductive coating used during FESEM study (Fig. 1b). Figure 1c, d shows the bright-field and dark-field TEM micrographs of the synthesized alumina powder which further endorsed the observation made during FESEM studies. The dark-field image (Fig. 1d) further illustrates the specific size range of the crystals through the presence of strongly illuminating nano-crystals of different shapes surrounded by relatively less brightened agglomerates which are mostly non-crystalline and non-Bragg diffracting.

Sintering of studied formulations

Figure 2a shows the morphology of as-received CNT with outer diameter of the nanotubes in the range of (59.06 ± 9.97) nm. It may be easily visualized from Fig. 2b that the nanotubes after SPS processing at 1500 °C under 40 MPa for 10 min suitably retained their morphology without any noticeable structural modification. Figure 3a, b shows the curves obtained during SPS processing of as-received MWCNT, pure α-Al2O3 and 0.25 and 0.5 wt% MWCNT/Al2O3 composites, respectively, to realize the nature of compaction and/or densification followed by the constituents and the composite. It is relevant to mention at this stage that the data acquisition software attached to the SPS furnace used in the present study recorded the SPS cycle parameters under pyrometer temperature sensing condition, i.e., 400 °C onward. Thus, under thermocouple temperature sensing (i.e., room temperature to 400 °C) the SPS cycle data were not recorded.

It may be easily understood from the figures that pure MWCNT underwent the least shrinkage (i.e., negligible densification) during the SPS cycle (Fig. 3b). For as-received CNT during the entire SPS process, both average piston speed and shrinkage remained almost constant at much lower values than those traced by the other specimens (Fig. 3a, b).

This was obvious because during SPS processing at 1500 °C under 40 MPa applied pressure, CNT being a sp^2-hybridized allotrope of carbon did not consolidate due to their extreme chemical inertness but only got compacted under the action of heat and

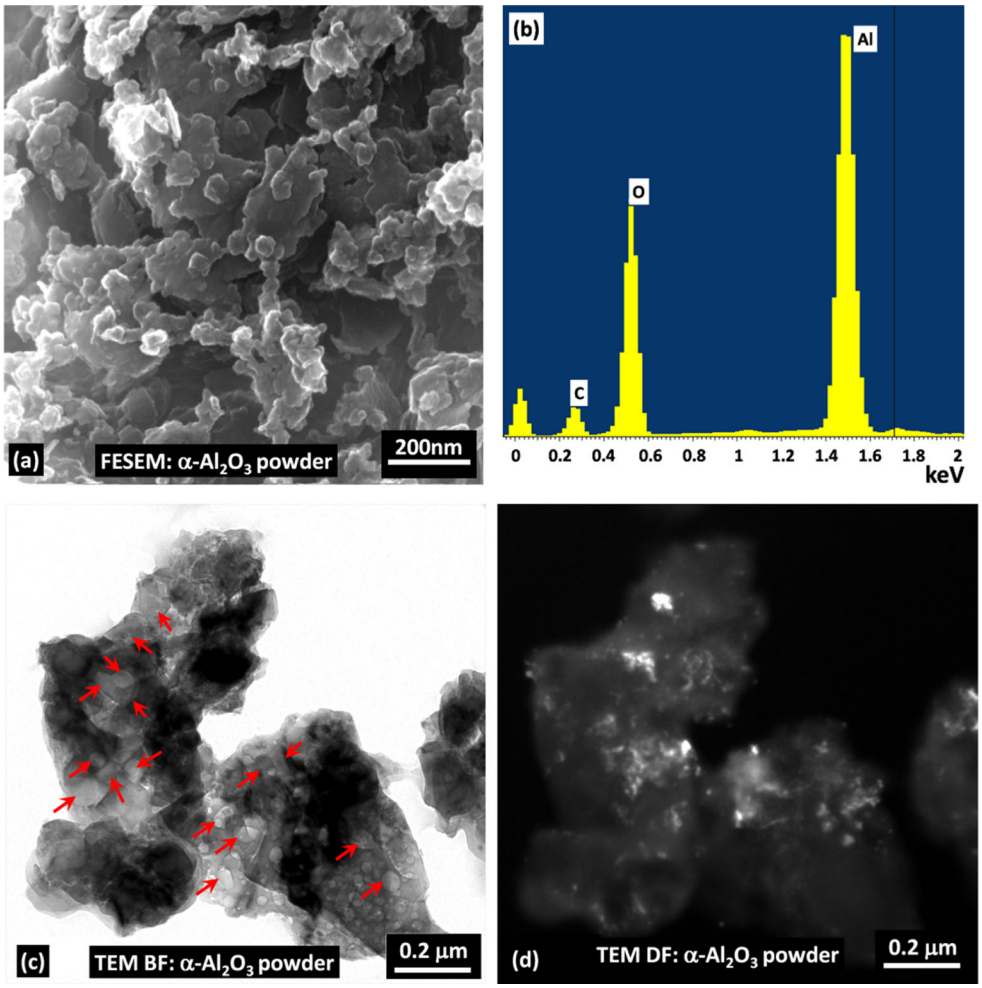

Figure 1 **a** FESEM image of heat-treated α-Al_2O_3 powder, **b** EDX pattern, **c, d** bright-field and corresponding dark-field images, respectively. Pointed arrows indicate existence of nano-grains within clustered regions.

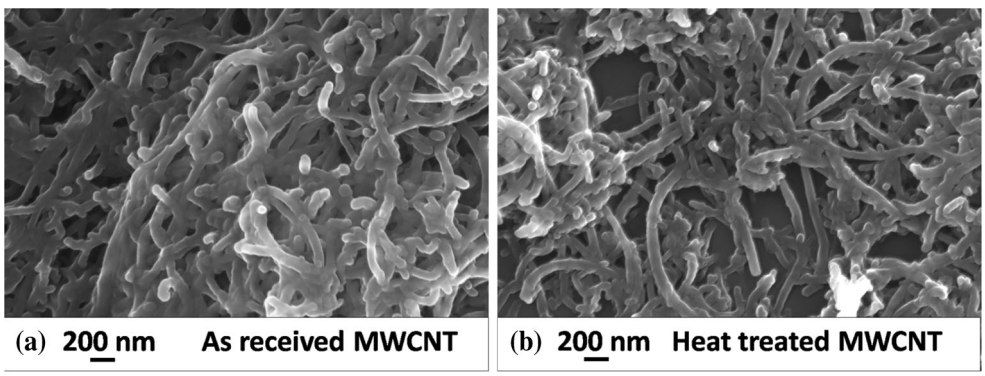

Figure 2 FESEM images of **a** as-received and **b** heat-treated MWCNT.

pressure. Furthermore, unlike CVD-grown individual MWCNT, when CNTs started to form bulk structures, e.g., bundles, sheets or layers, thermal diffusivity as well as conductivity values of the bulk structure decrease drastically. This happens primarily due to extensive phonon scattering through coupling between the nanotubes, structural defects like dangling bonds, tube ends and misalignment of CNTs in the bulk structure leading to as high as twelve times drop in the thermal diffusivity and

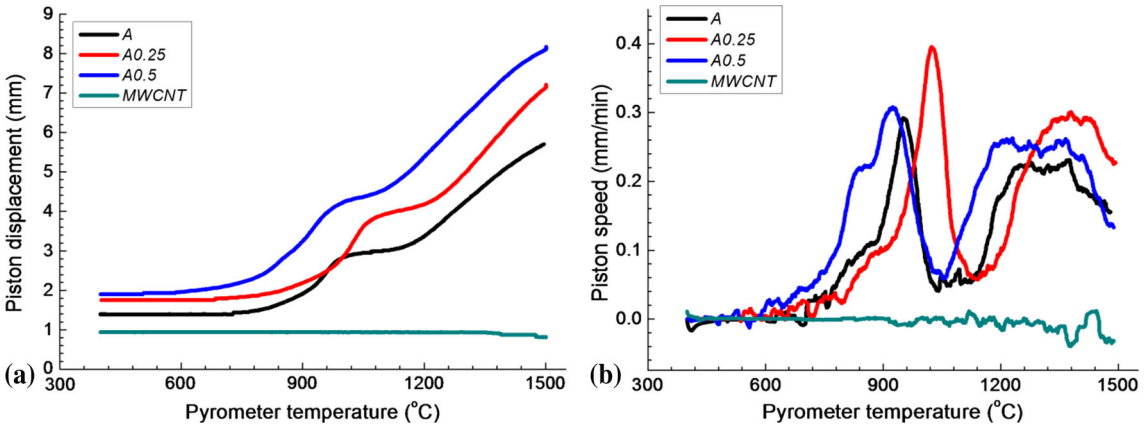

Figure 3 **a** Shrinkage versus pyrometer temperature plot and **b** rate of shrinkage versus pyrometer temperature plot for pure alumina, 0.25 and 0.5 wt% CNT containing composites and pure CNT during SPS processing at 1500 °C.

conductivity values compared to individual CNT [17]. Therefore, in the present study also, owing to the extremely flexible nature of CNT, compaction achieved under 40 MPa during the initial stage of SPS cycle, i.e., within 25 °C (start of the heating cycle) to 400 °C (temperature at which pyrometer started to measure the temperature replacing the thermocouple) significantly lowered the thermal diffusivity and conductivity values of the CNT bulk structure at later stage of the SPS cycle and, eventually, restricted further consolidation (i.e., shrinkage) to take place. However, structural purification of carbon nanotubes can take place at high temperature and/or under high pressure as reported by other researchers [18–21]. Due to this, the displacement curve as well as the shrinkage rate curve for MWCNT started from ~ 1 mm and ~ 0 mm/min, respectively and remained almost constant when the software started to record the SPS process parameters under pyrometer temperature sensing, i.e., from 400 °C onward (Fig. 3a, b). This indicated that the presence of ~ 5 wt% impurity (primarily metal catalyst particles or amorphous carbon) in as-received CNT did not form adequate liquid phase for further consolidation of the CNT compact. Nevertheless, after the consolidation process, the compacted CNT was obtained as a solid disk specimen and not in powdered form. The FESEM image shown in Fig. 2b was taken after crushing the SPS-processed compacted MWCNT in a mortar pestle followed by ultrasonic dispersion of a small amount from the crushed specimen in isopropyl alcohol. On the contrary, pure alumina and the composites underwent appreciable shrinkage, i.e., much enhanced densification (Fig. 3b) at comparatively much higher rate as illustrated in the piston speed versus temperature plot (Fig. 3a). The general features of the shrinkage curves are two distinct steps: the first one ending at temperatures on an average around 1000–1050 °C which is followed by the final rise through a plateau of around 250–300 °C in between the heating period. The rate curves accordingly produced two maxima, the first one in the range of 930–1020 °C and the second one ranging between 1340 and 1390 °C. To pursue the reasoning of the first maxima, a differential thermal analysis of the as-synthesized alumina was performed at an applied heating rate of 10 K min^{-1} (Fig. 4). An exothermic peak was obtained at 844 °C. X-ray diffraction results of heat treatment under different dwell times (figures not presented) proved that this temperature corresponded to the crystallization temperature of the amorphous variety. The observed first maximum in the sintering curve is therefore the consequence of crystallization of the amorphous portion of starting alumina. The drift in the maxima values from that of the DTA perhaps resulted from the combined effect of higher heating rate (i.e., 25 °C/min) and pressure used during the SPS process. The second maxima in the sintering curves, however, represent the highest rates of the compaction (i.e., densification) behavior of the individual compositions under study. Most interestingly, the onset temperatures of densification were found to be almost the same for pure alumina and the composites (Fig. 3a) though the composites offered higher shrinkage values than that obtained for the latter (Fig. 3b).

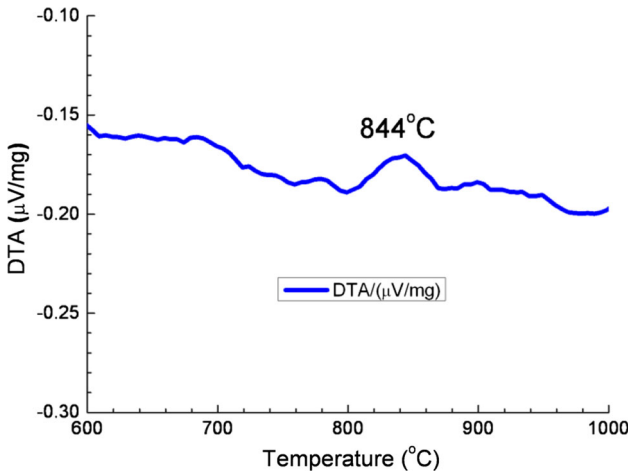

Figure 4 DTA of as-synthesized powder.

It is a well-known fact that CNT being one of the most chemically inert substances hinders grain boundary mass transport during sintering of CNT/Al_2O_3 composites [8, 22]. On the other hand, owing to exceptionally high electrical conductivity of CNT, its presence in the composite can also establish effective electrical conduction paths in otherwise highly insulating alumina matrix which in turn can render enhanced localized heating of the matrix grains, essentially, in the case of SPS processing where the consolidating powder can transmit electric current depending on its resistivity and resulted in better densification (i.e., higher shrinkage) [23–25]. The crystallization and densification processes are reflected in the trends shown in Fig. 3b. For 0.25 wt% MWCNT/Al_2O_3 composite, both the processes started at higher temperatures compared to pure alumina, while on the other hand, the opposite behaviors were shown by the 0.5 wt% MWCNT/Al_2O_3 composite. These happened because at lower CNT concentration, limited or no additional electrical conduction paths (electrical percolation) were established in insulating alumina matrix and presence of uniformly dispersed CNTs only restricted densification. However, as the temperature raised to the higher side, owing to the very high thermal conductivity (600 ± 100 W/m–K for individual MWCNT) [17], the presence of 0.25 wt% dispersed CNTs rendered improved localized heating of the matrix grains leading to higher densification compared to pure alumina or 0.5 wt% MWCNT/Al_2O_3 composite (Fig. 3b). On the contrary, at 0.5 wt% CNT loading, formation of additional electrical conduction paths through the insulating matrix combined with enhanced localized heating of the consolidating matrix facilitated faster onset of crystallization and densification compared to pure alumina and 0.25 wt% MWCNT/Al_2O_3 composite. Nevertheless, at 0.5 wt% CNT loading, the presence of exactly twofold higher concentration of nanotubes in alumina matrix might also hinder the densification process much severely compared to that happened for the 0.25 wt% MWCNT/Al_2O_3 composite. Therefore, both positive and negative effects of CNT incorporation in alumina matrix could have acted simultaneously during the SPS cycle and the trends obtained in the shrinkage curves (Fig. 3b) were the overall outcomes of those mutually contrasting processes, especially for the composites. Such reasoning is further reinstated because of the fact that shrinkage of the compact is increased with increasing CNT concentration in the composites (Fig. 3b). BD values of SPS-processed pure Al_2O_3 (~ 3.90 g/cc), 0.25 wt% (~ 3.87 g/cc) and 0.5 wt% MWCNT/Al_2O_3 composites (~ 3.85 g/cc) were found to be almost close to each other. This indicated the specimens were almost 98% dense considering the theoretical densities of Al_2O_3 and MWCNT as 3.97 and 1.8 g/cc, respectively [26–28]. Evidently, the present SPS schedule effectively could consolidate the MWCNT-reinforced combustion-synthesized nano-α-Al_2O_3 composite powder mixtures having density data equivalent or better than those achieved by others [7, 8, 11, 28].

Microstructure observation revealed formation of equiaxed grains in the sintered specimens (Fig. 5a–c). Owing to the characteristic nature of SPS technique, all the specimens showed controlled grain growth to produce a fine grain size distribution. While grain size of pure Al_2O_3 was found to be 1.55 ± 0.51 μm (Fig. 5a), addition of CNT resulted in further grain refinement and eventually, matrix grain sizes of 0.25 and 0.5 wt% MWCNT/Al_2O_3 composites were found to be 1.24 ± 0.20 and 1.01 ± 0.19 μm, respectively, with higher population of smaller sized grains (Fig. 5b, c). Beside this, Fig. 5b, c further shows bridging of multiple alumina grains by uniformly distributed and structurally survived CNTs in the composites.

Vickers hardness and ISE of the sintered specimens

The H_V values as a function of indentation load (P) of the sintered specimens are shown in Fig. 6a. Although H_V values of the sintered pure Al_2O_3

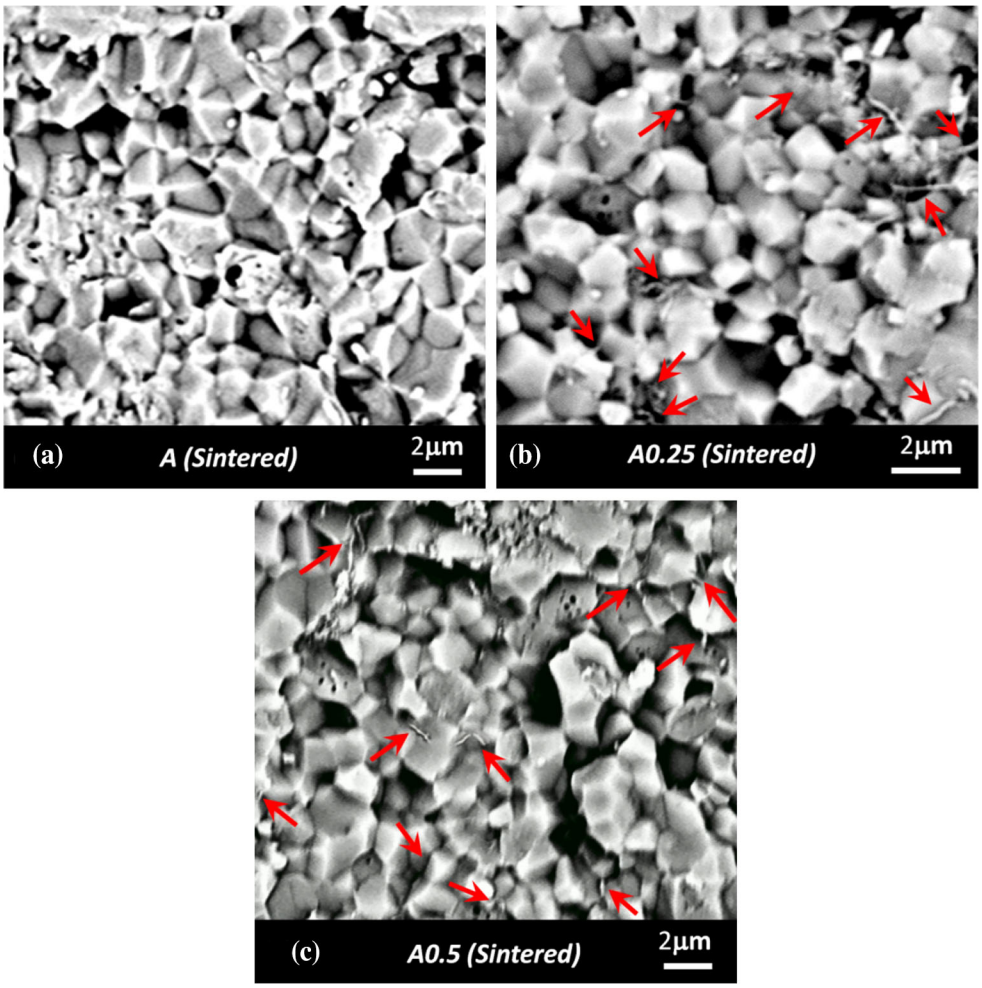

Figure 5 SEM images of SPS-processed **a** pure Al_2O_3; MWCNT/Al_2O_3 composite of **b** 0.25 wt%, **c** 0.5 wt%. Pointed arrows indicate well-distributed CNTs in the alumina matrix.

ranged from 20 to 19 GPa within the investigated loading range, composite containing 0.5 wt% MWCNT offered much higher H_V values from 24 to 21 GPa (Fig. 6a). Hardness values obtained for pure Al_2O_3 in this study were found to be on the higher side of available literature data. Additionally, enhancement in hardness (10–20%) values through MWCNT incorporation as obtained in the present study is also on the higher side when compared to the earlier literature [7–9, 11, 29]. Since hardness of polycrystalline material increases with decrease in the grain size of test material [9], higher H_V of present SPS-processed pure Al_2O_3 was principally obtained due to the starting nano-dimension of combustion-synthesized α-Al_2O_3 powder along with fast consolidation using SPS processing that restricted uncontrolled grain growth to produce a finer microstructure as shown in Fig. 5a. Reduction in H_V through MWCNT incorporation in Al_2O_3 matrices is a common issue, though [7, 9, 11, 29–35] improvement in H_V data of CNT/Al_2O_3 composites up to a certain concentration of CNT on the other hand has also been reported by a few researchers [8, 9, 36, 37]. The reasons behind obtaining reduced H_V through nanotube incorporation are, in general, the extreme flexible nature of CNT that facilitates higher permanent deformation of the surrounding matrix material, as well as a higher concentration induces inhomogeneous distribution of nanotubes in the matrix phase those act as defects of similar size [7, 11, 38]. On the contrary, improvement in H_V can be obtained firstly through uniform dispersion of CNT in the parent matrix by keeping the nano-filler concentration at a lower level to ensure proper densification of the composite, secondly by matrix–filler load sharing through proper interface region and thirdly by

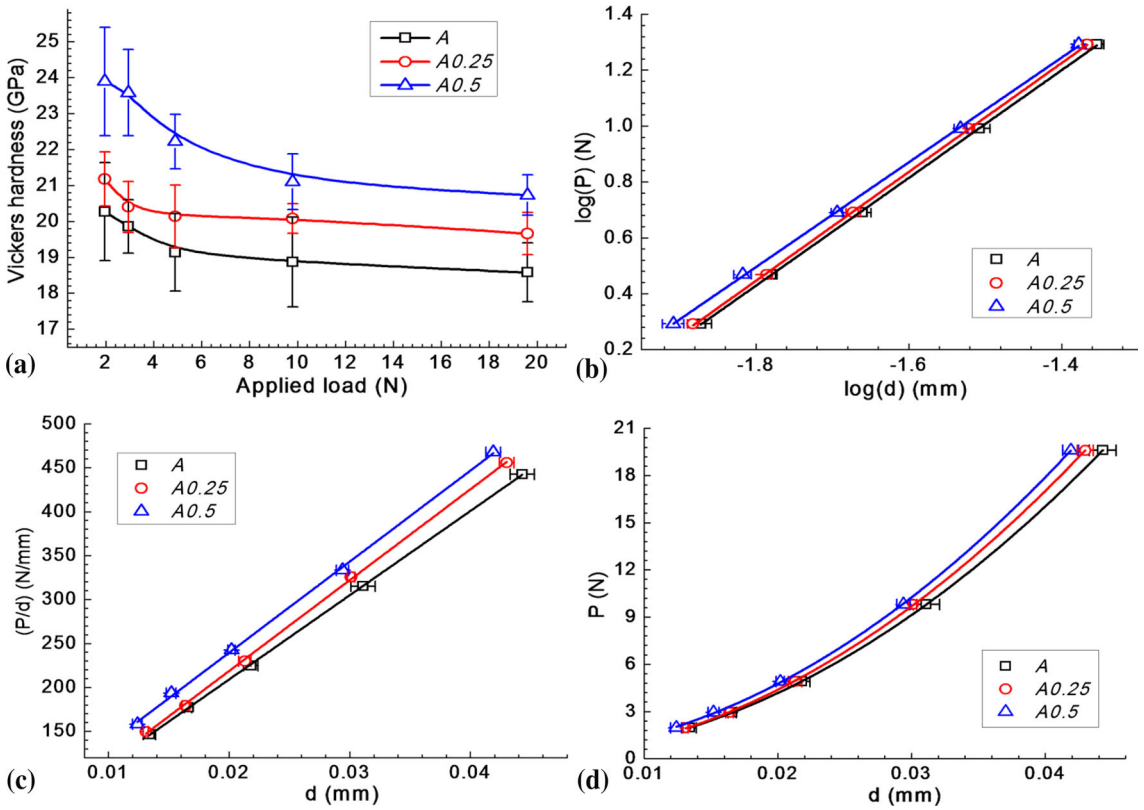

Figure 6 **a** Micro-Vickers hardness versus indentation load plot, **b** log(P) versus log(d) plot according to Meyer's law, **c** (P/d) versus d plot according to PSR model and **d** P versus d plot according to MPSR model of the studied specimens. 'P' and 'd' in the plots indicate indentation load and Vickers diagonal length, respectively.

imparting the well-known grain refining effect of CNT in Al_2O_3 to further reduce the matrix grain size [8, 36, 37]. Clearly, enhancement in H_V data of present MWCNT/Al_2O_3 composites may be ascribed to be achieved by the above factors. It may be further noted from Fig. 6a that all the specimens exhibited a decreasing H_V with increasing test load that indicates a normal indentation size effect. Thus, the experimental H_V data of all the specimens were analyzed with the help of three mathematical models namely Meyer's law, proportional specimen resistance (PSR) model and modified PSR (MPSR) model to quantitatively describe ISE of present samples [39, 40]. The plots according to Meyer's law, PSR and MPSR models of the studied specimens are shown in Fig. 6b–d, and the results obtained are given in Table 1. It may be understood from the Meyer's exponent value that pure Al_2O_3 and 0.25 wt% MWCNT/Al_2O_3 composite possessed almost similar sensitivity toward ISE with an exponent value close to 2 [40]; however, the sensitivity toward normal ISE of the 0.5 wt% MWCNT/Al_2O_3 composite was the highest (Table 1). Analogous to the Meyer's exponent result, the highest value of the 'a_1' term of A0.5 specimen as obtained from PSR model also indicated

Table 1 ISE analysis results of the SPS-processed specimens

Meyer's law results	*A*	A 0.25	A 0.5
Meyer's exponent (n)	1.927	1.947	1.874
R^2	0.999	0.999	0.999
PSR model results			
a_1 (N/mm)	17.25	11.86	32.21
a_2 (N/mm^2)	9586.79	10339.14	10362.05
R^2	0.999	0.999	0.999
$H_{T\text{-}PSR}$ (GPa)	17.77	19.17	19.22
MPSR model results			
P_0 (N)	0.09	− 0.09	0.22
a_1 (N/mm)	8.80	19.90	12.27
a_2 (N/mm^2)	9740.41	10196.67	10737.66
$H_{T\text{-}MPSR}$ (GPa)	18.06	18.91	19.91
R^2	0.999	0.999	0.999

'a_1' and 'a_2' are related to the proportional resistance and true hardness (H_T) of the test material, respectively. P_0 indicates machining-induced surface residual stress

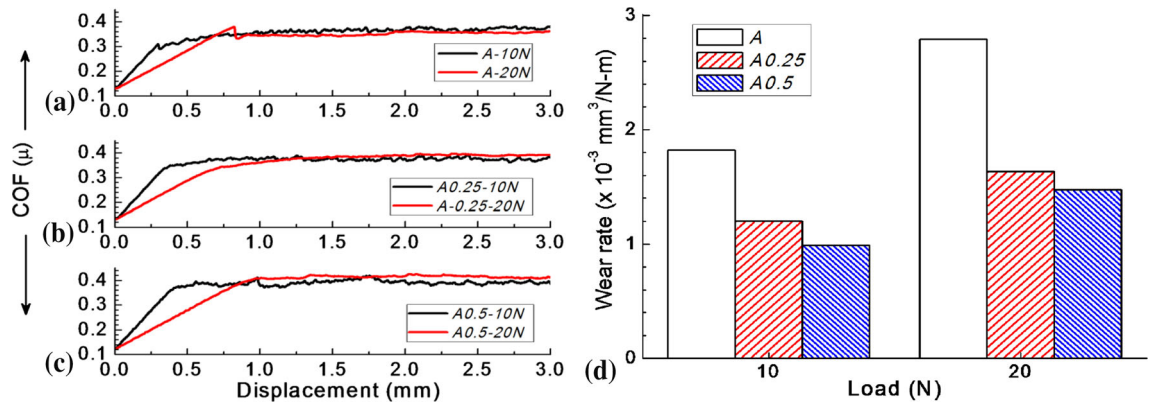

Figure 7 **a**–**c** COF values as a function of scratching distance and **d** specific wear rate versus normal load plot of the studied specimens.

the highest contribution to ISE (Table 1). On the contrary, the same specimen also exhibited the highest true hardness (a_2) within the investigated loading region. While the highest magnitude of H_T was obtained primarily due to adequate matrix densification, proper matrix–filler load sharing and formation of finer grains at 0.5 wt% CNT loading (Table 1), increasing indentation load resulted in enhanced probability of interaction with higher concentration of extremely flexible CNT in the matrix phase leading to a quick decline in H_V data.

Figure 6c shows the plots according to MPSR model and the results indicated formation of either negative (compressive) or positive (tensile) surface residual stress (P_0) in the studied specimens (Table 1). Since the magnitude of the residual stress was found to be low enough (< 0.3), its effect on hardness value may be treated as negligible. Present results on quantitative analyses of ISE matched well with the available literature data on ISE for monolithic as well as CNT-reinforced alumina ceramics prepared by different techniques [40].

Unlubricated wear characteristics of the sintered specimens

Surface roughness (Ra) values of the polished samples were measured as < 0.14 μm. The COF versus distance plots for the studied specimens are shown in Fig. 7a–c. Irrespective of the specimen composition and test load, magnitude of the COF value ranged between 0.37 and 0.42 that matched well with results obtained by others [13–15].

Although it was reported that addition of 0.3 wt% graphene nano-platelet and 1 wt% MWCNT resulted in ~ 12% reduction in COF of a hybrid Al_2O_3 composite due to higher toughness and easy debundling of CNT in the presence of the nano-platelets [10], in present study, reinforcement of Al_2O_3 with up to 0.5 wt% CNT did not help much in reducing the COF of the composites by imparting its self-lubrication property. However, considering the nature of the COF curves, it may be stated that the indenter tip–specimen interaction was reasonably regular that resulted in almost unaltered steady state COF values throughout the scratching process (Fig. 7a–c). Figure 7d shows the W_R values of the studied specimens as a function of test load. CNT-reinforced composites offered much improved wear resistance against the diamond indenter than that obtained for SPS-processed pure Al_2O_3 (Fig. 7d). Evidently, grain boundary strengthening (20–35% reduction in matrix grain size was obtained for the composites through addition of carbon nanotubes), and improved hardness and effective bridging of matrix grains through structurally survived CNTs (Fig. 5b, c) that rendered suitable toughening effect were the key factors behind obtaining such improved wear resistance of the composites. Depending on test loads, while the 0.25 wt% MWCNT/Al_2O_3 specimen offered ~ 34–42% lower W_R values compared to monolithic Al_2O_3(^{10N} $W_R \approx 1.8 \times 10^{-3}$ mm^3/N-m; ^{20N} $W_R \approx 2.8 \times 10^{-3}$ mm^3/N-m), composite containing 0.5 wt% CNT offered more than 45% lower W_R values than that obtained for pure Al_2O_3 (Fig. 7d). Scar profile observation using SEM revealed large uncovered areas of mixed mode (i.e., transgranular–intergranular) fracture in the wear track of pure Al_2O_3 (Fig. 8a, b). On the contrary, formation of tribofilm of increasing thickness with increased CNT loading was noticed in the wear tracks of composite specimens (Fig. 8c–f). The tribofilm possibly formed

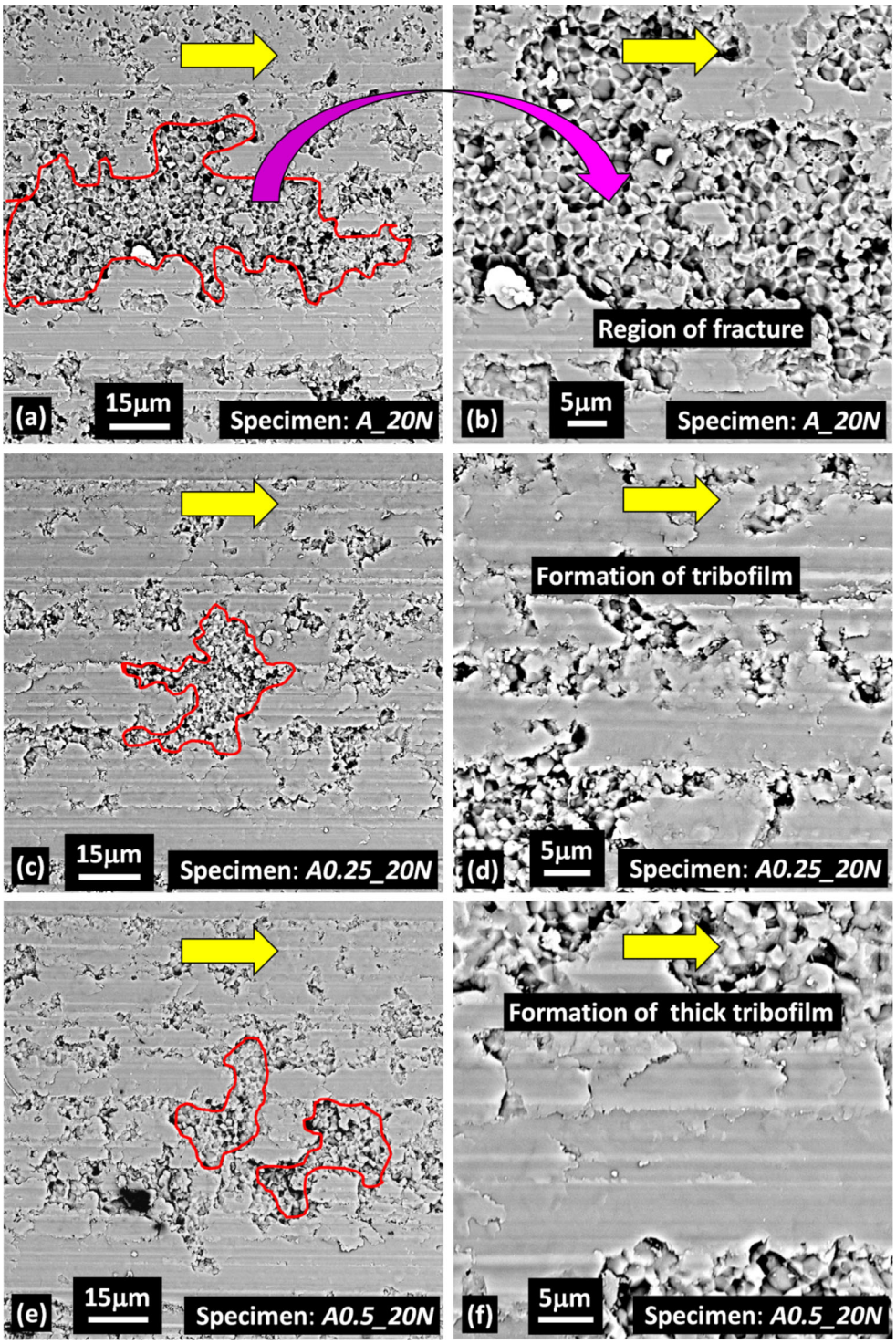

Figure 8 Wear track profiles of **a, b** pure Al_2O_3 showing large unwrapped regions of mixed mode fracture, **c, d** 0.25 wt% MWCNT/Al_2O_3 composite, **e, f** 0.5 wt% MWCNT/Al_2O_3 composite, showing gradually reduced area of unwrapped fractured surface and formation of thicker tribofilm under F_N = 20 N.

out of crushing of the pulled out matrix grains and nanotubes under the test load. Formation of such adhered tribofilm of increasing thickness with increasing CNT loading restricted further material removal during the scratching event for the composite specimens [10].

Conclusions

Using gel-combustion processing, 30–70 nm sized fully pure α-Al_2O_3 powder was synthesized. This laboratory-made powder and its composites with different concentration of commercial MWCNT were sintered under SPS processing at 1500 °C to near theoretical density values within only 10 min. Sintering is influenced sequentially by the crystallization of the amorphous alumina followed by the diffusion process. The sintering curves indicate the positive effect of CNT incorporation that provides localized conducting paths in otherwise electrically non-conducting alumina toward achieving better densification compared to the monolithic. The composites containing up to 0.5 wt% nanotubes showed formation of fine microstructure comprising of ~ 1-μm-sized equiaxed grains and uniformly distributed structurally survived CNTs in the matrix phase. The maximum H_V values at 0.2 and 2 kgf indentation loads obtained for 0.5 wt% MWCNT/Al_2O_3 composite were ~ 18 and ~ 12% higher, respectively, than those measured for pure Al_2O_3($H_{V0.2}$ ≈ 20 GPa; H_{V2} ≈ 18.6 GPa). ISE analyses revealed that the magnitude of true hardness of 0.5 wt% CNT/Al_2O_3 composite ($H_{T\text{-}PSR}$ ≈ 19.2 GPa; $H_{T\text{-}MPSR}$ ≈ 20 GPa) was the highest among the studied specimens. Additionally, the highest sensitivity toward size effect was also observed for the same composite due to enhanced interaction with extremely flexible CNTs at higher loads. Beside adequate densification, improved hardness, proper bridging of multiple matrix grains by well-dispersed nanotubes to ensure the expected toughening mechanisms to take place, formation of an adhered tribofilm within the wear track of the composites at the initial stage of scratching event offered nearly 30–45% lower specific wear rate values compared to SPS-processed monolithic alumina.

Acknowledgements

The first author conveys sincere thanks to CSIR for Research Associate position. Helps from the institutional characterization units are gratefully acknowledged. Thanks are due to the Director of CSIR-Central Glass & Ceramic Research Institute, for his interest.

Funding

This study was funded by Council of Scientific and Industrial Research (CSIR), India (Grant Number: MLP-0202).

Compliance with ethical standards

Conflicts of interest The authors have no conflicts of interest related to this work.

References

[1] Milak PC, Minatto FD, De Noni G Jr., Montedo ORK (2015) Wear performance of alumina-based ceramics—a review of the influence of microstructure on erosive wear. Cerâmica 61:88–103

[2] Al-Sanabani FA, Madfa AA, Al-Qudaimi NH (2014) Alumina ceramic for dental applications: a review article. Am J Mater Res 1:26–34

[3] Silva MV, Stainer D, Al-Qureshi HA, Montedo ORK, Hotza D (2014) Alumina-based ceramics for armor application: mechanical, characterization and ballistic testing. J Ceram 2014:618154

[4] da Costa Evangelista JP, Gondim AD, Di Souza L, Araujo AS (2016) Alumina-supported potassium compounds as heterogeneous catalysts for biodiesel production: a review. Renew Sustain Energy Rev 59:887–894

[5] Munro RG (1997) Evaluated material properties for a sintered α-alumina. J Am Ceram Soc 80:1919–1928

[6] Galusek D, Galusková D (2015) Alumina matrix composites with non-oxide nanoparticle addition and enhanced functionalities. Nanomaterials 5:115–143

[7] Bocanegra-Bernal MH, Dominguez-Rios C, Echeberria J, Reyes-Rojas A, Garcia-Reyes A, Aguilar-Elguezabal A (2016) Spark plasma sintering of multi-, single/double-and single-walled carbon nanotube-reinforced alumina composites: is it justifiable the effort to reinforce them? Ceram Int 42:2054–2062

[8] Ahmad K, Pan W (2015) Microstructure-toughening relation in alumina based multiwall carbonnanotube ceramic composites. J Eur Ceram Soc 35:663–671

[9] Yazdani B, Xia Y, Ahmad I, Zhu Y (2015) Graphene and carbon nanotube (GNT)-reinforced alumina nanocomposites. J Eur Ceram Soc 35:179–186

[10] Yazdani B, Xu F, Ahmad I, Hou X, Xia Y, Zhu Y (2015) Tribological performance of graphene/carbon nanotube hybrid reinforced Al_2O_3 composites. Sci Rep 5:11579

[11] Gallardo-López A, Poyato R, Morales-Rodríguez A, Fernández-Serrano A, Munoz A, Domı´nguez-Rodríguez A

(2014) Hardness and flexural strength of single-walled carbon, nanotube/alumina composites. J Mater Sci 49: 7116–7123. https://doi.org/10.1007/s10853-014-8419-5

[12] Sarkar S, Das PK (2012) Microstructure and physicomechanical properties of pressureless sintered multiwalled carbon nanotube/alumina nanocomposites. Ceram Int 38: 423–432

[13] An J-W, You D-H, Lim D-S (2003) Tribological properties of hot-pressed alumina–CNT composites. Wear 255: 677–681

[14] Lim D-S, You D-H, Choi H-J, Lim S-H, Jang H (2005) Effect of CNT distribution on tribological behavior of alumina–CNT composites. Wear 259:539–544

[15] Kim SW, Chung WS, Sohn K-S, Son C-Y, Lee S (2010) Improvement of wear resistance in alumina matrix composites reinforced with carbon nanotubes. Metall Mater Trans A 41A:380–388

[16] Halder R, Bandyopadhyay S (2017) Synthesis and optical properties of anion deficient nano MgO. J Alloys Compd 693:534–542

[17] Aliev AE, Lima MH, Silverman EM, Baughman RH (2010) Thermal conductivity of multi-walled carbon nanotube sheets: radiation losses and quenching of phonon modes. Nanotechnology 21:035709

[18] Kajiura H, Tsutsui S, Huang H, Murakami Y (2002) High-quality single-walled carbon nanotubes from arc-produced soot. Chem Phys Lett 364:586–592

[19] Suzuki T, Inoue S, Ando Y (2008) Purification of single-wall carbon nanotubes by using high-pressure micro reactor. Diam Relat Mater 17:1596–1599

[20] Bertoncini M, Coelho LAF, Maciel IO, Pezzin SH (2011) Purification of single-wall carbon nanotubes by heat treatment and supercritical extraction. Mater Res 14:380–383

[21] Sarkar S, Das PK (2013) Thermal and structural stability of single- and multi-walled carbon nanotubes up to 1800 °C in Argon studied by Raman spectroscopy and transmission electron Microscopy. Mater Res Bull 48:41–47

[22] Hanzel O, Sedlácek J, Sajgalík P (2014) New approach for distribution of carbon nanotubes in alumina matrix. J Eur Ceram Soc 34:1845–1851

[23] Ando Y, Zhao X, Shimoyama H, Sakai G, Kaneto K (1999) Physical properties of multiwalled carbon nanotubes. Int J Inorganic Mater 1:77–82

[24] McEuen PL, Fuhrer MS, Park H (2002) Single-walled carbon nanotube electronics. IEEE Trans Nanotechnol 1:78–85

[25] Huang Q, Jiang D, Ovidko IA, Mukherjee A (2010) High-current-induced damage on carbon nanotubes: the case during spark plasma sintering. Scripta Mater 63:1181–1184

[26] Yamamoto G, Omori M, Yokomizo K, Hashida T (2008) Mechanical properties and structural characterization of carbon nanotube/alumina composites prepared by precursor method. Diam Relat Mater 17:1554–1557

[27] Bi S, Hou G, Su X, Zhang Y, Guo F (2011) Mechanical properties and oxidation resistance of α-alumina/multi-walled carbon nanotube composite ceramics. Mater Sci Eng, A 528:1596–1601

[28] Bi S, Su X, Hou G, Liu C, Song W-L, Cao M-S (2013) Electrical conductivity and microwave absorption of shortened multi-walled carbon nanotube/alumina ceramic composites. Ceram Int 39:5979–5983

[29] Kasperski A, Weibel A, Estournès C, Laurent Ch, Peigney A (2013) Preparation-microstructure-property relationships in double-walled carbon nanotubes/alumina composites. Carbon 53:62–72

[30] Michálek M, Sedláček J, Parchoviansky M, Michálková M, Galusek D (2014) Mechanical properties and electrical conductivity of alumina/MWCNT and alumina/zirconia/MWCNT composites. Ceram Int 40:1289–1295

[31] Bakhsh N, Khalid FA, Hakeem AS (2013) Synthesis and characterization of pressureless sintered carbon nanotube reinforced alumina nanocomposites. Mater Sci Eng, A 578:422–429

[32] Puchy V, Hvizdos P, Dusza J, Kovac F, Inam F, Reece MJ (2013) Wear resistance of Al_2O_3–CNT ceramic nanocomposites at room and high temperatures. Ceram Int 39:5821–5826

[33] Thomson KE, Jiang D, Yao W, Ritchie RO, Mukherjee AK (2012) Characterization and mechanical testing of alumina-based nanocomposites reinforced with niobium and/or carbon nanotubes fabricated by spark plasma sintering. Acta Mater 60:622–632

[34] Zhang SC, Fahrenholtz WG, Hilmas GE, Yadlowsky EJ (2010) Pressureless sintering of carbon nanotube–Al_2O_3 -composites. J Eur Ceram Soc 30:1373–1380

[35] Jiang D, Thomson K, Kuntz JD, Ager JW, Mukherjee AK (2007) Effect of sintering temperature on a single-wall carbon nanotube-toughened alumina-based nanocomposite. Scripta Mater 56:959–962

[36] Echeberria J, Rodríguez N, Vleugels J, Vanmeensel K, Reyes-Rojas A, Garcia-Reyes A, Domínguez-Rios C, Aguilar-Elguézabal A, Bocanegra-Bernal MH (2012) Hard and tough carbon nanotube-reinforced zirconia-toughened alumina composites prepared by spark plasma sintering. Carbon 50:706–717

[37] Ahmad I, Unwin M, Cao H, Chen H, Zhao H, Kennedy A, Zhu YQ (2010) Multi-walled carbon nanotubes reinforced Al_2O_3 nanocomposites: mechanical properties and interfacial investigations. Compos Sci Technol 70:1199–1206

[38] Aguilar-Elguézabal A, Bocanegra-Bernal MH (2014) Fracture behaviour of α-Al_2O_3 ceramics reinforced with a mixture of single-wall and multi-wall carbon nanotubes. Compos Part B 60:463–470

[39] Li H, Bradt RC (1993) The microhardness indentation load/size effect in rutile and cassiterite single crystals. J Mater Sci 28:917–926. https://doi.org/10.1007/BF00400874

[40] Gong J, Wu J, Guan Z (1999) Examination of the indentation size effect in low-load vickers hardness testing of ceramics. J Eur Ceram Soc 19:2625–2631